JACS
JOURNAL OF THE AMERICAN CHEMICAL SOCIETY

COMMUNICATION

pubs.acs.org/JACS

Comparison of Solution and Crystal Structures of PreQ$_1$ Riboswitch Reveals Calcium-Induced Changes in Conformation and Dynamics

Qi Zhang,[†] Mijeong Kang,[†,‡] Robert D. Peterson,[†,‡] and Juli Feigon*[,†,‡]

[†]Department of Chemistry and Biochemistry and [‡]UCLA−DOE Institute for Genomics and Proteomics, University of California, Los Angeles, California 90095-1569, United States

Supporting Information

ABSTRACT: Riboswitches regulate gene expression via specific recognition of cognate metabolites by their aptamer domains, which fold into stable conformations upon ligand binding. However, the recently reported solution and crystal structures of the *Bacillus subtilis* preQ$_1$ riboswitch aptamer show small but significant differences, suggesting that there may be conformational heterogeneity in the ligand-bound state. We present a structural and dynamic characterization of this aptamer by solution NMR spectroscopy. The aptamer−preQ$_1$ complex is intrinsically flexible in solution, with two regions that undergo motions on different time scales. Three residues move in concert on the micro-to-millisecond time scale and may serve as the lid of the preQ$_1$-binding pocket. Several Ca^{2+} ions are present in the crystal structure, one of which binds with an affinity of 47 ± 2 μM in solution to a site that is formed only upon ligand binding. Addition of Ca^{2+} to the aptamer−preQ$_1$ complex in solution results in conformational changes that account for the differences between the solution and crystal structures. Remarkably, the Ca^{2+} ions present in the crystal structure, which were proposed to be important for folding and ligand recognition, are not required for either in solution.

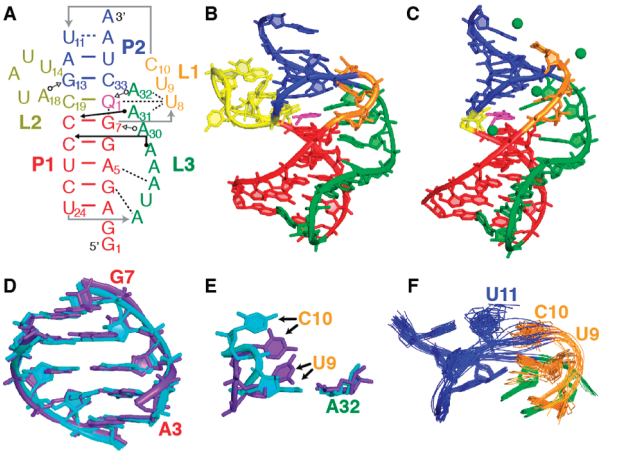

Figure 1. Comparison of solution and crystal structures of the *B. subtilis* preQ$_1$ riboswitch aptamer−preQ$_1$ complex. Shown are the (A) secondary, (B) lowest-energy solution (PDB ID 2L1V), and (C) crystal (PDB ID 3K1V) structures of the complex. Four Ca^{2+} in the crystal structure are shown as green spheres. (D) Overlay of P1 from the solution (purple) and crystal (cyan) structures after P1−L3 superposition. (E) Overlay of U9, C10, and A32 from the solution (purple) and crystal (cyan) structures after P2−L1 superposition. (F) Conformations of U9, C10, and U11 in the solution structures.

Riboswitches are an important class of regulatory RNA elements that are found in the 5′ untranslated regions of some mRNAs and usually consist of an aptamer and an expression platform.[1] Specific binding of a small metabolite to the aptamer leads to rearrangement of the secondary structure of the riboswitch, and the resultant conformational change in the expression platform turns gene expression on or off at either the transcriptional or translational level. Over the last six years, high-resolution structures of aptamers from 12 classes of riboswitches have been determined, providing significant insights into how they recognize their cognate metabolites.[2−5] Although conformational rearrangements are one of the hallmarks of riboswitches,[6−12] the conformations of the ligand-bound aptamer appear to be highly stable on the basis of the crystal structures. However, the stabilities of these aptamer−ligand complexes are difficult to evaluate from structures directly, as almost all of them were solved by X-ray crystallography, where the sample conditions as well as RNA sequences were optimized to form well-ordered crystals. We recently reported the first solution structure of a riboswitch aptamer, the *Bacillus subtilis* preQ$_1$ riboswitch aptamer in complex with the preQ$_1$ ligand. The preQ$_1$ riboswitch has the smallest known natural aptamer domain and modulates biosynthesis of queuosine (Q) by recognizing the Q precursor 7-aminomethyl-7-deazaguanine (preQ$_1$).[13−17] The *B. subtilis* preQ$_1$ riboswitch aptamer is also the only one for which both solution and crystal structures have been determined.[15,16] The detailed comparison of these two structures presented here has revealed small but significant conformational differences in the positions of residues above the binding pocket, suggesting conformational heterogeneity in the ligand-bound state.[18] Using solution-NMR approaches, we investigated the conformational plasticity of the riboswitch in the ligand-bound state and evaluated the effects of crystallization conditions on riboswitch structure and dynamics.

The secondary structure of the *B. subtilis* preQ$_1$ riboswitch aptamer is a hairpin with an A-rich tail.[13] In the presence of preQ$_1$, the A-rich tail base-pairs with the nucleotides in the center of the hairpin loop to form an H-type pseudoknot with two helices (P1 and P2) and three loops (L1, L2, and L3)

Received: December 31, 2010
Published: March 16, 2011

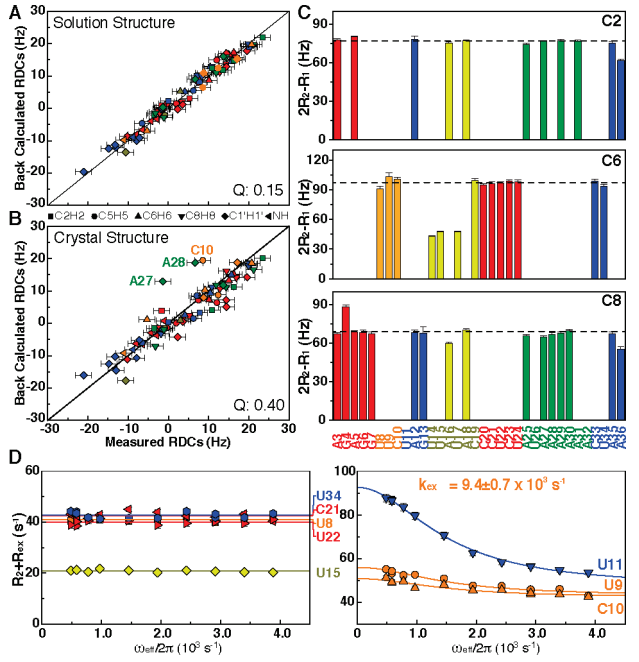

Figure 2. Structural dynamics of the *B. subtilis* preQ$_1$ riboswitch aptamer−preQ$_1$ complex. (A, B) Correlation between measured and back-calculated RDCs using (A) the lowest-energy solution structure and (B) the crystal structure. Symbols are colored as the secondary structure. (C) Dynamics on the ps−ns time scale. Shown are values of $2R_2 - R_1$ for C2, C6, and C8 derived from R_1 and $R_{1\rho}$ measurements at a field strength of 800 MHz. Dashed lines are the average values excluding L2 residues. (D) Dynamics on the μs−ms time scale. Shown are the effective spin-lock-field dependences of $R_2 + R_{ex}$ for base carbons C6 at a field strength of 600 MHz. The solid lines represent the best fits of the relaxation rates using the fast-exchange equation. The relaxation rates of U9, C10, and U11 were fitted globally to a single exchange rate.

(Figure 1A). In most H-type pseudoknots, L2 has 0−2 nucleotides (nts). In the preQ$_1$-bound aptamer, L2 is unusually long, with 6 nts, the last of which stacks on P1 to base-pair with preQ$_1$. Our previously reported NMR solution structure was determined primarily with nuclear Overhauser effect (NOE)-derived distances and experimentally derived dihedral angles.[16] To have a high-precision comparison between the solution and crystal structures, we first rerefined the solution structure with an extensive set of residual dipolar couplings (RDCs) [Table S1 in the Supporting Information (SI)].[19,20] A few additional NOE restraints were also obtained and incorporated into the structure calculations during this refinement. The ensemble of the rerefined 20 lowest-energy structures was better determined with an rmsd to the mean of 0.64 ± 0.13 Å (PDB ID 2L1V).

A comparison of the lowest-energy solution structure[16] and the highest-resolution crystal structure (PDB ID 3K1V)[15] is shown in Figure 1. Despite the different sample conditions and experimental approaches, the lower regions of the aptamer (P1, L3, and residue C19 from L2) in the two structures are nearly identical, with an rmsd of 1.2 ± 0.1 Å for the all-heavy-atom superposition (Figure 1D), including the presence of unusual A-amino hydrogen bonds between L3 residues and the minor groove of P1 (A-amino kissing motif).[16] However, there are some interesting differences in the remaining regions of the aptamer. First, there is a sharp turn at the end of L1 in the crystal structure, with the last nucleotide C10 involved in a noncanonical base pair with A35 at the top of P2. This results in a more compact L1−P2 loop, with a closer approach of the phosphodiester backbones of L1 and P2 than in the solution structure. In addition, there is a Hoogsteen U9−A32 base pair in the crystal structure. In contrast, C10 is not stacked on P2, and the positions of U9, C10, and U11 are less well-defined in the solution structures (Figure 1F). Thus, the upper region of the crystal structure (P2 and L1) differs significantly from that of the solution structure, with an rmsd of 2.0 ± 0.1 Å for the all-heavy-atom superposition (Figure 1E). Second, all of the crystal structures of the aptamer (two L2 sequence variants and different structures in the asymmetric units) have several visible Ca^{2+}. In the highest-resolution structure there are four Ca^{2+} ions, two in the L1−P2 turn and two at the interface between aptamers in the asymmetric unit (Figure 1C). However, Ca^{2+} is not present in the solution study. Third, while L2 is reasonably well-defined in the solution structures, none of the L2 residues except for the last one, which is hydrogen-bonded to preQ$_1$, are visible in the highest-resolution crystal structure. In the lower-resolution crystal structures, three L2 residues are not visible.

To verify that the conformational similarities and differences between the solution and crystal structures were not due to differences in structure refinement protocols, we performed a direct order tensor analysis of the experimental RDCs of both structures.[20] Since RDCs were used in refining the solution structure, they fit excellently to the solution structure with a Q factor[21] of 0.15, as expected (Figure 2A). However, the measured RDCs did not agree well with values back-calculated from the crystal structure (Q = 0.40) (Figure 2B), confirming the presence of conformational differences between the crystal and solution structures. Fitting of RDCs to the P1/L3 residues confirmed that the lower regions of the aptamer in the crystal and solution structures are almost identical, with the exception of the C1′H1′ bonds from L3 residues A27 and A28 (Figure S1 in the SI), which adopt significantly different orientations in the crystal and solution structures. These differences can be attributed to the movement of L3 as a consequence of Ca^{2+} binding. Excluding the RDCs for A27 and A28 C1′H1′ gave Q = 0.21 when 39 RDCs were fitted to P1/L3 (Figure S1). However, even after exclusion of these two RDCs either alone or with another major outlier (C5H5 of C10), the back-calculated RDCs from the entire crystal structure still showed discrepancies from the measured values (Q = 0.31 or 0.26, respectively). This is primarily due to different local conformations across P2/L1 rather than different relative orientations of P1/L3 and P2/L1 in the crystal and solution structures. Fitting 32 RDCs to P2/L1 in the crystal structure gave Q = 0.32 without major outliers (Figure S1). Thus, the RDC analysis shows that the conformational differences in P2/L1 in the crystal and solution structures are indeed significant. It further shows that most of P1/L3 is identical in solution and the crystal, illustrating that an NMR solution structure of RNA can be determined with an accuracy comparable to that for a high-resolution crystal structure given a sufficient number and accuracy of NOE and RDC restraints.

We next investigated the conformational flexibility of the riboswitch aptamer in the ligand-bound state on pico- to nanosecond (ps-ns) time scale using NMR relaxation measurements.[22,23] Analysis of the spin relaxation data (Figure 2C) revealed that L2 is the only highly dynamic region of the preQ$_1$-bound aptamer, which is consistent with the absence of most of the L2 residues in the crystal structures because of disorder.[15] Within this flexible loop, A18 and C19 are relatively rigid because of direct hydrogen bonding with G13 and preQ$_1$

dx.doi.org/10.1021/ja111769g |*J. Am. Chem. Soc.* 2011, 133, 5190–5193

respectively, while U14, U15, and U17 undergo the most significant local motions of all the residues in the aptamer. The remaining L2 residue, A16, shows limited flexibility, which may be largely due to its stacking interaction with A18. The rest of the aptamer residues, except for the terminal residue A36, also have limited motions on this time scale. It was somewhat surprising that the L1 residues U9 and C10, which have the largest conformational differences from the crystal structure and are among the least well-defined residues in solution, are remarkably stable on this time scale.

We further extended the dynamic characterization from the ps−ns to the μs−ms time scale and focused on regions with the largest conformational differences between the solution and crystal structures by applying a 1D-selective $R_{1\rho}$ experiment on individually U- and C-labeled samples [Figure 2D; also see Supporting Material and Methods (SMM) in the SI].[24] Stable residues residing within helices (C21, U22, and U34) all showed spin-lock-field-independent relaxation rates of base carbons C6, providing internal controls for the absence of conformational exchange. The much smaller relaxation rates for L2 residue U15 are consistent with its significant local dynamics on the ps−ns time scale, while the flat dispersion profile indicates that it has no motions on the longer μs−ms time scale. Residue U8 from L1, which forms a direct hydrogen bond with preQ$_1$, is also very stable on this time scale. In contrast, the relaxation dispersion profiles for C6s in U9, C10, and U11 revealed a very different map of dynamics in the RNA. These residues have prominent spin-lock-field-dependent relaxation rates, indicating that they undergo conformational exchange on the μs−ms time scale. Consistent with this, their positions were less well-defined by the NMR data. The individual dispersion profiles were fitted to the fast-exchange equation, which showed similar exchange rates (k_{ex} = 9−14 × 10^3 s^{-1}) (Figure S2). These residues are contiguous in sequence, but their backbones form a turn (Figure 1F) and their dispersion profiles could be globally fit to a single exchange rate of (9.4 ± 0.7) × 10^3 s^{-1} (Figure 2D), suggesting that they undergo concerted motions. We propose that during binding of preQ$_1$, these residues act as the lid of the binding pocket to sequester preQ$_1$ by properly positioning A12 and G13 to facilitate formation of P2.

In solution, the preQ$_1$ riboswitch aptamer folds and binds tightly to preQ$_1$ in the absence of Ca^{2+} or other divalent cations. In the crystal structures of the *B. subtilis* preQ$_1$ aptamer, there are 2−5 Ca^{2+} per aptamer, but only the one located at the sharp turn is shared in common among all crystal forms.[15] This Ca^{2+} has been proposed to stabilize the sharp turn at C10 present in the crystal structure, while the Ca^{2+} at the P1/P2 junction has been proposed to play a role in ligand binding by providing a water of hydration to form a hydrogen bond with preQ$_1$.[15] To investigate whether Ca^{2+} also binds to the preQ$_1$ aptamer in solution, we monitored chemical shift changes in $^1H-^{13}C$ HSQC spectra as a function of added Ca^{2+} up to a final amount of 10 equiv of Ca^{2+} (SMM and Figure S3). Figure 3A shows the chemical shift mapping onto the solution structure at 2 equiv of Ca^{2+}. The major chemical shift changes are localized in the L1/P2 region, which corresponds to the location of the Ca^{2+} found in common for all crystal forms, as well as where the major conformational differences between the solution and crystal structures were observed. These chemical shift changes reflect changes in the chemical environment due to either direct Ca^{2+} binding or Ca^{2+}-induced conformational changes. Fitting the chemical shift changes as a function of Ca^{2+} concentration gave values of the apparent dissociation constant (K_d) ranging from 3 to 734 μM

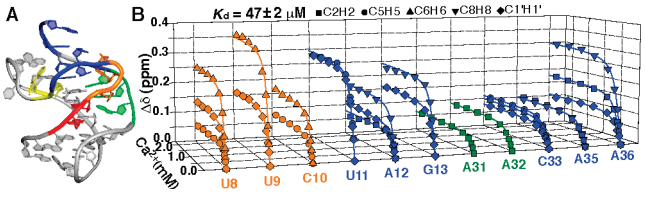

Figure 3. The *B. subtilis* preQ$_1$ riboswitch aptamer−preQ$_1$ complex has a high-affinity Ca^{2+} binding site in solution. (A) Chemical shift mapping of Ca^{2+} binding. Residues with >0.05 ppm chemical shift changes at 2 equiv of Ca^{2+} are highlighted in color on the structure. (B) Titration curves for the upper-domain residues as functions of Ca^{2+} concentration, yielding an apparent K_d of 47 μM from a global fit.

(SMM and Figure S4). These K_d values are clustered into two ranges, and interestingly, the residues falling in these two ranges are located either above or below the preQ$_1$-binding pocket, respectively (Figure S4). Global fitting of the chemical shift changes from these two clusters gave K_d values of 47 ± 2 and 361 ± 22 μM (Figure 3B and Figure S4).

Within the region of larger K_d (weaker binding), G7 and U14 have the biggest chemical shift changes, indicating the biggest influence of local environments upon Ca^{2+} binding (Figure S3). These two residues are next to the location of the Ca^{2+} in the crystal structure whose water of hydration forms a hydrogen bond with preQ$_1$. The weaker Ca^{2+} binding affinity at this location may explain why this Ca^{2+} was observed only in the highest-resolution crystal structure.[15] It also raises the possibility that this Ca^{2+} does not make a significant contribution to ligand binding. The sharp turn in L1−P2 binds Ca^{2+} much more tightly, with an order of magnitude higher affinity, consistent with the fact that the Ca^{2+} located at the sharp turn is shared in common among all of the crystal structures. We note that no chemical shift changes in the aptamer were observed when Ca^{2+} was added in the absence of preQ$_1$. Thus, these two Ca^{2+} binding sites are created only upon binding of preQ$_1$ to the aptamer. In contrast, in the TPP riboswitch, a high-affinity (K_d = 170 μM) divalent cation (Mg^{2+}) is a prerequisite for TPP binding.[25] In addition, the tight binding site is specific for Ca^{2+} and not for Mg^{2+}, as only minor chemical shift changes were observed upon titration with Mg^{2+} (Figure S5).

Since the preQ$_1$-bound aptamer tightly binds Ca^{2+} in solution, we hypothesized that the presence of Ca^{2+} in the crystallization condition might account for the conformational differences between the solution and crystal structures. To test this hypothesis, we measured RDCs in the preQ$_1$-bound aptamer in the presence of 6 mM Ca^{2+}. The 84 RDCs shared in common for the preQ$_1$-bound aptamer with and without Ca^{2+} were poorly correlated (R = 0.83) (Figure S6). The order tensor analysis showed that while the RDCs measured in the presence of Ca^{2+} did not fit well with the solution structure (Q = 0.34), they fit excellently with the crystal structure (Q = 0.19) (Figure 4 A,B). These results indicate that Ca^{2+} binding does induce conformational changes in the Ca^{2+}-free solution structure of the aptamer toward a conformation more similar to the crystal structure. Order tensor analysis of RDCs with individual domains showed that the structural changes are located in the P2/L1 region (Figure S7), and the poor correlation between the RDCs measured with and without Ca^{2+} is largely due to the changes in the overall alignment upon addition of Ca^{2+} (Table S5). Along with the structural changes, the dynamic properties of some residues in P2/L1 were also perturbed upon Ca^{2+} binding. On the ps−ns time scale, most residues do not experience

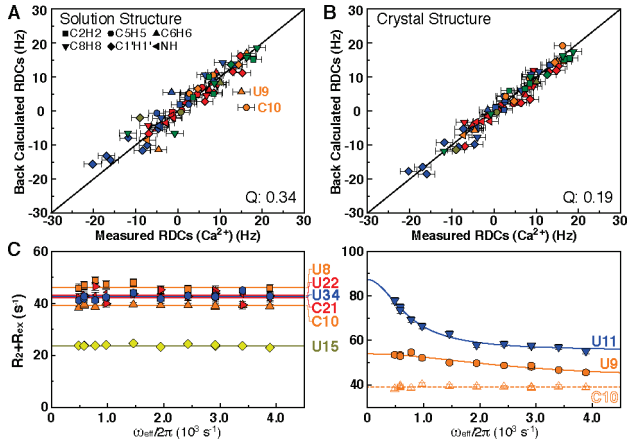

Figure 4. Calcium binding induces changes in the structure and dynamics of the *B. subtilis* preQ$_1$ riboswitch aptamer−preQ$_1$ complex. (A, B) Correlation between measured RDCs in the presence of 6 mM Ca^{2+} and values back-calculated using (A) the lowest-energy solution structure and (B) the crystal structure. (C) Dynamics of the aptamer−preQ$_1$ complex on the μs−ms time scale in the presence of 6 mM Ca^{2+}. Shown are the effective spin-lock-field dependences of $R_2 + R_{ex}$ for base carbons C6 at a field strength of 600 MHz, and solid lines represent the best fits of the relaxation rates. In the right panel, the relaxation dispersion profile of C10 is shown using open symbols for comparison.

significant changes in local dynamics, but C10, which caps P2 in the crystal structure, becomes more flexible (Figure S8). On the μs−ms time scale, the concerted motion of the lid is disrupted by Ca^{2+} binding. While the conformational exchange of C10 on the μs−ms time scale is completely quenched, U9 retains its exchange rate of $(16.1 \pm 4.6) \times 10^3\ s^{-1}$. Consistent with stabilization of P2 by Ca^{2+}, the exchange rate for P2 residue U11 decreases to a lower value of $(4.5 \pm 0.6) \times 10^3\ s^{-1}$ (Figure 4C).

In summary, we have shown that small but significant differences between the NMR solution and crystal structures of RNA can be accurately determined and evaluated. The observed conformational differences between the solution and crystal structures of the *B. subtilis* preQ$_1$ riboswitch aptamer, located in the upper stem, are largely due to the presence of Ca^{2+} in the crystallization conditions. While formation of a stable upper stem would appear to be important on the basis of the crystal structure alone, the solution structure and dynamics showed that the preQ$_1$ is tightly bound even with an apparently unstable upper stem. PreQ$_1$ is likely captured as the riboswitch RNA is being transcribed, and our results support the hypothesis that the concerted movement of the lid may function to capture preQ$_1$ prior to complete formation of the upper stem. Moreover, our structural and dynamic studies uncovered a Ca^{2+}-binding pocket that remarkably forms only upon ligand binding. Despite the apparent contribution (based on the crystal structure) of one of the bound Ca^{2+} to ligand recognition and the other to stable aptamer folding, the solution data revealed that they are not required for either. While the possibility of a functional role of Ca^{2+} in locking down the lid is intriguing, it seems unlikely because the resting concentration of Ca^{2+} in bacteria is 0.1−0.3 μM.[26] Even if activation up-regulates Ca^{2+} concentration by 10−100 fold, it would still be low relative to K_d. Divalent cations are frequently required for RNA folding and ligand binding,[27] so it is noteworthy that we have observed this case of fortuitous formation of a divalent-cation binding pocket in the crystal structure that is most likely not essential in vivo.

■ ASSOCIATED CONTENT

Supporting Information. Sample preparation, experimental procedures, and additional results. This material is available free of charge via the Internet at http://pubs.acs.org.

■ AUTHOR INFORMATION

Corresponding Author
feigon@mbi.ucla.edu

■ ACKNOWLEDGMENT

This work was supported by grants from DOE, NSF, and NIH to J.F. Q.Z. is a Baltimore Family Fellow of the Life Sciences Research Foundation.

■ REFERENCES

(1) Roth, A.; Breaker, R. R. *Annu. Rev. Biochem.* **2009**, *78*, 305.
(2) Montange, R. K.; Batey, R. T. *Annu. Rev. Biophys.* **2008**, *37*, 117.
(3) Serganov, A.; Patel, D. J. *Biochim. Biophys. Acta* **2009**, *1789*, 592.
(4) Zhang, J.; Lau, M. W.; Ferre-D'Amare, A. R. *Biochemistry* **2010**, *49*, 9123.
(5) Huang, L.; Serganov, A.; Patel, D. J. *Mol. Cell* **2010**, *40*, 774.
(6) Buck, J.; Furtig, B.; Noeske, J.; Wohnert, J.; Schwalbe, H. *Proc. Natl. Acad. Sci. U.S.A.* **2007**, *104*, 15699.
(7) Greenleaf, W. J.; Frieda, K. L.; Foster, D. A.; Woodside, M. T.; Block, S. M. *Science* **2008**, *319*, 630.
(8) Ali, M.; Lipfert, J.; Seifert, S.; Herschlag, D.; Doniach, S. *J. Mol. Biol.* **2010**, *396*, 153.
(9) Baird, N. J.; Ferre-D'Amare, A. R. *RNA* **2010**, *16*, 598.
(10) Lee, M. K.; Gal, M.; Frydman, L.; Varani, G. *Proc. Natl. Acad. Sci. U.S.A.* **2010**, *107*, 9192.
(11) Stoddard, C. D.; Montange, R. K.; Hennelly, S. P.; Rambo, R. P.; Sanbonmatsu, K. Y.; Batey, R. T. *Structure* **2010**, *18*, 787.
(12) Duchardt-Ferner, E.; Weigand, J. E.; Ohlenschlager, O.; Schmidtke, S. R.; Suess, B.; Wohnert, J. *Angew. Chem., Int. Ed.* **2010**, *49*, 6216.
(13) Roth, A.; Winkler, W. C.; Regulski, E. E.; Lee, B. W.; Lim, J.; Jona, I.; Barrick, J. E.; Ritwik, A.; Kim, J. N.; Welz, R.; Iwata-Reuyl, D.; Breaker, R. R. *Nat. Struct. Mol. Biol.* **2007**, *14*, 308.
(14) Meyer, M. M.; Roth, A.; Chervin, S. M.; Garcia, G. A.; Breaker, R. R. *RNA* **2008**, *14*, 685.
(15) Klein, D. J.; Edwards, T. E.; Ferre-D'Amare, A. R. *Nat. Struct. Mol. Biol.* **2009**, *16*, 343.
(16) Kang, M.; Peterson, R.; Feigon, J. *Mol. Cell* **2009**, *33*, 784; Erratum:**2010**, *39*, 653.
(17) Spitale, R. C.; Torelli, A. T.; Krucinska, J.; Bandarian, V.; Wedekind, J. E. *J. Biol. Chem.* **2009**, *284*, 11012.
(18) Bailor, M. H.; Musselman, C.; Hansen, A. L.; Gulati, K.; Patel, D. J.; Al-Hashimi, H. M. *Nat. Protoc.* **2007**, *2*, 1536.
(19) Tjandra, N.; Bax, A. *Science* **1997**, *278*, 1111.
(20) Prestegard, J. H.; Al-Hashimi, H. M.; Tolman, J. R. *Q. Rev. Biophys.* **2000**, *33*, 371.
(21) Cornilescu, G.; Bax, A. *J. Am. Chem. Soc.* **2000**, *122*, 10143.
(22) Hansen, A. L.; Al-Hashimi, H. M. *J. Am. Chem. Soc.* **2007**, *129*, 16072.
(23) Dethoff, E. A.; Hansen, A. L.; Musselman, C.; Watt, E. D.; Andricioaei, I.; Al-Hashimi, H. M. *Biophys. J.* **2008**, *95*, 3906.
(24) Hansen, A. L.; Nikolova, E. N.; Casiano-Negroni, A.; Al-Hashimi, H. M. *J. Am. Chem. Soc.* **2009**, *131*, 3818.
(25) Yamauchi, T.; Miyoshi, D.; Kubodera, T.; Nishimura, A.; Nakai, S.; Sugimoto, N. *FEBS Lett.* **2005**, *579*, 2583.
(26) Dominguez, D. C. *Mol. Microbiol.* **2004**, *54*, 291.
(27) Draper, D. E. *Biophys. J.* **2008**, *95*, 5489.